Weierstraß–Institut
für Angewandte Analysis und Stochastik

Modeling of Self-Pulsating DFB Lasers

M. Radziunas[1,2], H.-J. Wünsche [2], B. Sartorius [3], O. Brox[3],

D. Hoffmann[3], K. Schneider[1]

submitted: 3rd September 1999

[1] Weierstraß-Insitut für Angewandte
     Analysis und Stochastik,
     Mohrenstraße 39, 10117 Berlin, Germany
     E-Mail: radziuna@wias-berlin.de,
     schneider@wias-berlin.de

[2] Institut für Physik
     der Humboldt-Universität zu Berlin,
     Invalidenstr. 110, 10115 Berlin, Germany
     E-Mail: wuensche@physik.hu-berlin.de

[3] Heinrich-Hertz-Institut für Nachrichtentechnik Berlin,
     Einsteinufer 37, D-10587 Berlin, Germany
     E-Mail: sartorius@hhi.de, brox@hhi.de, hoffmann@hhi.de

Abstract

A theoretical model of a self-pulsating three section DFB-laser with an integrated phase tuning section is established. It is based on traveling wave equations and the standard carrier rate equations. As the key conditions for obtaining self-pulsations the spectral correlation of the different device sections are considered. The specific roles of each section are discussed and the theoretical results are compared to experimental measurements on these devices.

1 Introduction

High-speed self-pulsations (SP) of multi-section DFB lasers were discovered in 1992 [1]. Until now repetition frequencies up to $80\,GHz$ were reported, tunable by the injected currents [2]. This has opened a new field for the optical clock recovery at high bit rates. All-optical clock recovery could be demonstrated with such devices [3, 4] in wavelength and polarization independent operation. Its system capability has been demonstrated as well[5, 6, 7]. The clock modules can replace the electronic clock recovery and furthermore since the clock signal is in the optical domain it can be used as control signal for all-optical demultiplexers.
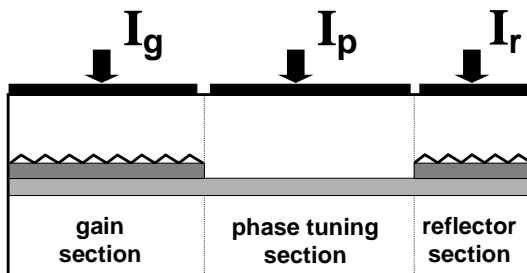
Fig. 1: Scheme of the device with the integrated passive phase tuning section in the center.

Two-section DFB-devices have been investigated in experiment and theory in different laboratories. Measurements showed quite a variety of results regarding the conditions for generating DFB-type SP and regarding the achieved device properties. SP below 5 GHz were found in a few laboratories [8, 9, 10], while high-speed SP were reported only from the Heinrich-Hertz-Institute [2] for some selected devices.

Different possible SP mechanisms have been proposed in the published modeling work. Among these was spatial hole burning (SHB) [11, 12, 13], dispersive self Q-switching (DQS) [14, 13, 15, 16] and mode beating [15, 16]. A direct comparison with measurements was impossible because devices fabricated with apparently identical parameters exhibited very different SP phenomena. This is mainly due to the scatter in the positions of the laser facets relative to the Bragg grating, which cannot be controlled during the fabrication process.

Reproducible high-speed SP of the DQS type could be achieved by introducing an additional phase-tuning section between the DFB-sections and the facet [17, 18]. Good qualitative and quantitative agreement of the single-mode model of DQS with measurements was demonstrated for this type of devices [19].

The present generation of devices has a further modified structure ([20], Fig. 1). It is completely AR-coated and consists of two DFB sections and one phase section integrated in between. The two DFB sections are basically identical, only lengths and pump levels are different. The longer one is pumped highly $j = 14kA/cm^2$ and provides the gain for lasing in the $1.5\,\mu m$ spectral range. The shorter DFB section is driven close to its gain transparency $j = 2kA/cm^2$ and acts as the dispersive reflector. The center section has no grating. Its $1.3\,\mu m$ active layer does not couple to the $1.5\,\mu m$ laser emission. It serves as the passive phase tuning section. Accordingly, quantities referring to the gain, phase and reflector sections will be labeled by g, p and r, respectively.

In this paper, we present for the first time modeling results for this new device generation with an improved model. We demonstrate that this model describes in good correspondence with the experiments the main features of the new device generation.

The structure of the paper is as follows. Section 2 describes the model which is based on travelling wave and carrier rate equations. In section 3 the basic conditions for self-pulsations are shown and compared to experimental results. Section 4 is dedicated to the role of the phase current. In section 5 two main function of the gain current are discussed. Finally the conclusions are summarized in section 6.

2   Model and Parameter Description

There are several possibilities of modeling the temporal behaviour of DFB lasers. Existing dynamic models are based, for example, on the solution of the dynamic coupled wave equation using transfer-matrix method [21], [24], the power-matrix method [23] or finite difference methods in time domain [22].

To model dispersive self-Q-switching in DFB lasers, a single-mode approximation of traveling wave equations was also successfully used [15], [19]. Our calculations are based on Finite Difference solution of the equations in the time domain and are also compared with an Transfer Matrix approach described in [24, 13].

2.1   Traveling Wave Equations (TWE)

Supposing stable index guiding in the fundamental TE mode, the optical field within the laser is the superposition of two counter-propagating waves in a small spectral interval around the central wavelength $\lambda_0 \approx 1.5\,\mu m$. The slowly varying amplitudes

$\Psi^{\pm}(z, t)$ of these waves obey the well known traveling wave equations (TWE) [25]

$$
\begin{aligned}
\left(-i v_{group}^{-1} \partial_t - i \partial_z + \beta\right) \Psi^+ + \kappa^+ \Psi^- &= F_{sp}^+ \\
\left(-i v_{group}^{-1} \partial_t + i \partial_z + \beta\right) \Psi^- + \kappa^- \Psi^+ &= F_{sp}^-,
\end{aligned}
\tag{1}
$$

where ∂_t and ∂_z are the partial derivatives with respect to time t and position z, respectively. The group velocity v_{group}, and the coupling coefficients κ^+ and κ^- of the Bragg gratings are constant within each section. For the index grating of our device it holds $\kappa^- = (\kappa^+)^*$. Because of the AR coating of the facets and the tunable phase shift in the phase section between the two DFB's, the phases of κ play no role and we use real positive values estimated from the measured stop band widths.

$\beta(z, t)$ is the propagation constant of the local waveguide at the central wavelength minus the reference value π/Λ determined by the unique corrugation period Λ of the Bragg sections. In each section we consider

$$
\beta(z, t) = \delta - i \frac{\alpha_0}{2} + (\alpha_H + i) \frac{\Gamma g(z, t)}{2}
\tag{2}
$$

with the material gain in the active zone AZ

$$
g(z, t) = g' [N(z, t) - N_{tr}].
\tag{3}
$$

The parameters $\alpha_0, \alpha_H, \Gamma, g'$, and N_{tr} represent the internal optical losses, Henry's linewidth enhancement factor, the transverse modal fill factor, the differential gain, and the transparency concentration, respectively, of the corresponding section. δ is a static detuning parameter to be specified in the subsequent chapters.

The quantities $F_{sp}^{\pm}$ in Eq. (1) represent the Langevin noise sources due to spontaneous emission. They are simulated in accordance with the quantum properties of light by appropriate sequences of random numbers as described in [24]. We have found that the impact of spontaneous emission on the self-pulsations of the considered device is negligible, as was already observed for two-section lasers in [15]. As a consequence, we shall not discuss in detail this part of the model. All examples presented below have been calculated without spontaneous emission, for simplicity.

The TWE represent hyperbolic partial differential equations. They have to be completed by initial and boundary conditions. We use reflecting boundary conditions

$$
\Psi^+(0, t) = r_0 \Psi^-(0, t) \quad \text{and} \quad \Psi^-(L, t) = r_L \Psi^+(L, t)
\tag{4}
$$

at the facets $z = 0$ and $z = L$ of the device. Considering AR coated devices only, the amplitude facet reflectivities r_0 and r_L are set to zero in this paper. The initial conditions for $\Psi^{\pm}$ are of minor importance if a unique and stable stationary or self-pulsating final lasing state exists that is always achieved after some relaxation oscillations. Our measurements, however, indicated the appearance of hysteresis and multistability under certain conditions. For finding such effects in the modeling, we have applied different initial conditions for the same set of parameters. More details will be discussed in chapter 4.

2.2 Carrier Rate Equations

The relative propagation constants depend parametrically on the longitudinal position z and on time instant t via the carrier density $N(z,t)$. Therefore, the optical TWE have to be coupled with a carrier equation. Neglecting effects of Spatial Hole Burning, the carrier rate equation

$$\frac{\partial}{\partial t}N = \frac{I}{ewdl} - R(N) - \Gamma v_g g S. \tag{5}$$

can be used. Here we suppose that $N(z,t)$ are spatially constant in each of laser sections and the quantity

$$S(z,t) = \frac{1}{wdl}\int_{\nu \in (L_k \ni z)}\left(|\Psi^+(\nu,t)|^2 + |\Psi^-(\nu,t)|^2\right)d\nu \tag{6}$$

is the mean photon density governing the stimulated emission. Here w, d, l are width, thickness and length of the AZ in the corresponding section. By normalization, $|\Psi^\pm(z,t)|^2$ is the number of photons (field energy / $\hbar\omega_0$) per unit length in the forward / backward traveling wave. Notice that this expression does not contain the rapidly varying standing wave patterns corresponding to the mixed terms of $|E(z,t)|^2$.

All possible further recombination channels are summarized in the second term, which is parametrized as usual in the polynomial form

$$R(N) = AN + BN^2 + CN^3. \tag{7}$$

In the first term of (5), e is the electron charge and I represents the current injected into the respective section.

2.3 Numerics

To solve equations 1 – 5 we have used two different numerical schemes.

The first one is a second order accuracy finite difference scheme for solving the TWE (1) and carrier rate equation (5) in time domain.

After discretization of spatial domain $z \in [0;L]$ with uniform steps h we take the step of time domain τ satisfying the relation $\tau = v_g^{-1}h$. Moreover, we require that each of the laser sections contain integer number of spatial steps. Now for each grid point $(z,t) \in [0,L) \times [0,T)$ we denote

$$\tilde{\Psi}^+ = \left(\Psi^+(z+h,t+\tau) + \Psi^+(z,t)\right)/2, \quad \tilde{\Psi}^- = \left(\Psi^+(z,t+\tau) + \Psi^+(z+h,t)\right)/2,$$

$$S\left(t,z+\frac{h}{2}\right) = \frac{h}{wdl}\sum_{\nu+h/2\in(L_k\ni z+h/2)}\left(|\Psi^+(\nu,t)|^2 + |\Psi^-(\nu+h,t)|^2\right),$$

$$\tilde{N} = \frac{1}{2}\left(N\left(z+\frac{h}{2},t+\tau\right) + N\left(z+\frac{h}{2},t\right)\right), \quad \tilde{S} = \frac{1}{2}\left(S\left(z+\frac{h}{2},t+\tau\right) + S\left(z+\frac{h}{2},t\right)\right)$$

4

and write the finite difference schemes as follows:

$$\Psi^+(z+h,t+\tau) - \Psi^+(z,t) = -ih\left(\beta\left(\tilde{N}\right)\tilde{\Psi}^+ + \kappa\tilde{\Psi}^-\right)$$
$$\Psi^-(z,t+\tau) - \Psi^+(z+h,t) = -ih\left(\beta\left(\tilde{N}\right)\tilde{\Psi}^- - \kappa\tilde{\Psi}^+\right)$$
$$N(z+h/2,t+\tau) - N(z+h/2,t) = \tau\left(I/(ewdl) - R\left(\tilde{N}\right) - \Gamma v_g g\left(\tilde{N}\right)\tilde{S}\right).$$

Solving these nonlinear equations at the beginning we predict the values of carrier densities at the new time level $t+\tau$. For this reason we use the values of photon densities in stimulated emission term and the values of carrier densities in recombination term at the time level t. Afterwards we explicitly compute the values of optical fields at the time moment $t+\tau$ and then correct the values of carrier densities at the same time moment.

The second numerical scheme is based on the transfer-matrix method for the hyperbolic PDE (1) as described in [24] combined with the forward Euler method for the carrier rate equation (5). This method was already successfully applied for describing the SP of two-section devices [13], showing good agreement with the single mode model [15].

Comparable results were obtained with both schemes. In both methods, the discretization of the time - space domain is the same. The following results for the $750\,\mu m$ long device have been obtained with 50 spatial steps. Computations with greater number of spatial steps showed similar results.

In the computations we used the following values of the parameters mentioned above: $\kappa_{g,r}^+ = \kappa_{g,r}^- = 180\,cm^{-1}$, l_g, l_p, $l_r = 300,\ 300$ and $150\,\mu m$, $c/v_{group} = 3.4$, $\Gamma = 0.3$, $g'_{g,r} = 3\cdot 10^{-16}\,cm^2$, $N_{tr} = 10^{18}\,cm^{-3}$, $\alpha_H = -8$, $\alpha_{0,g}$, $\alpha_{0,p}$, $\alpha_{0,r} = 25,\ 20$ and $25\,cm^{-1}$, $d = 0.15\,\mu m$, $w = 3\,\mu m$, $A = 3\cdot 10^8\,s^{-1}$, $B = 10^{-10}\,cm^3 s^{-1}$, $C = 10^{-28}\,cm^6 s^{-1}$.

The values of other parameters are subject for changes and will be discussed below in the paper.

3 Basic Conditions for Self-Pulsations

Both in experiment and theory, the basic requirement for DQS-SP is operation above threshold and a specific spectral correlation between the stop bands of the two DFB sections as depicted by the reflectivity spectra in Fig. 2. The resonance "ear" of the highly pumped gain section, which indicates the lasing mode, has to be somewhere on the right decaying slope of the reflector section spectrum.

Experimentally, the relative spectral position of the stop band of the gain section is adjusted by the gain current I_g, keeping the reflector at transparency. For I_g just at the laser threshold, an electronic blue-shift of about -2nm can be determined from the ASE spectra. This is much too large for observing SP. Fortunately, the blue-shift reduces with increasing I_g and the desired spectral situation is achieved in the range of 90 mA. This effect can be attributed to the heating of the gain section.

From independent measurements, we got typically about 0.02 nm thermal red-shift per mA gain section current.
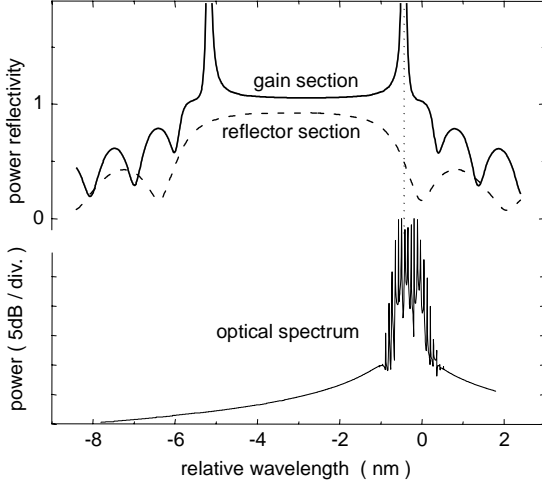
Fig. 2: Calculated spectra of a typical self-pulsating state for $I_g = 90$ mA and appropriate detuning and phase conditions. Thin: spectrum of the optical output at the gain section facet. Thick: the corresponding feedback spectra of the reflector section (full) and of the gain section (dashed) for one moment during the SP.
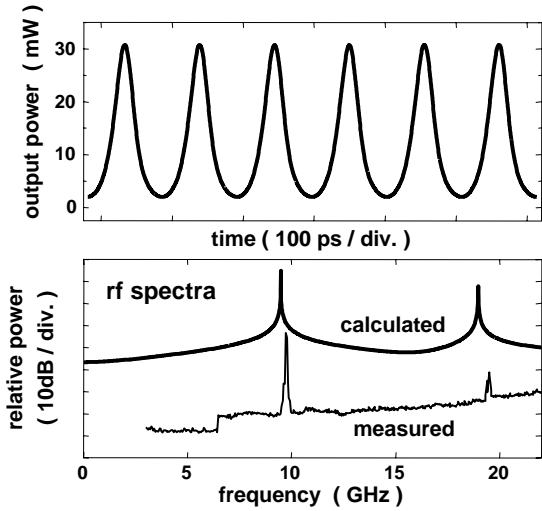
Fig. 3: Pulse traces and rf spectra of a free running SP corresponding to the situation of Fig.2. Solid: calculated. Dashed: measured.

In the model, the relative position of the two stop bands is determined by the differences between the real parts of β in the two DFB sections. According to Eq. (2), $\Re\{\beta\}$ has a static contribution δ and an electronic contribution $\alpha_H \Gamma g/2$. In the reflector section we set $\delta = 0$ by appropriately fixing the reference wavelength λ_0. Furthermore, the electronic contribution is also negligible due to pumping close to transparency. Thus, the spectral correlation of the two stop bands is mainly determined by the $\Re\{\beta\}$ of the gain section. The electronic contribution is negative and yields about $2\,nm$ blue-shift for a typical threshold concentration of $1.5 \times 10^{18}\ cm^{-3}$, in good coincidence with the measurements. The measured thermal red shift corresponds to a static contribution $\delta = 50\,A^{-1}(I - I_{tr})/l$ to β [19]. This yielded the spectral situation of Fig. 2 for a current of $90\,mA$. For an appropriate phase condition (cf. next section), we get SP for these currents both in theory and experiment. The calculated pulse power trace of the optical output at the gain facet of the laser is drawn Fig. 3 showing well modulated self-pulsations. In the experiments, a direct measurement of pulse traces was not possible with an oscilloscope since the phase of subsequent pulses is not correlated. However, after conversion of the optical power fluctuations with an HP 11982A light wave converter into the electrical domain the SP could be recorded with an HP 8593A electrical spectrum analyzer.

The appearance and the frequencies of SP were deduced from rf spectra as depicted in the lower part of Fig. 3. The step in rel. power at $6.5\,GHz$ results from the transition to a second local oscillator within the used instrument. Theoretical power

spectra were computed using discrete FFT from the pulse power trace showing good agreement experimental results. The basic frequencies are close to each other. Furthermore, the ratio between the two harmonics is also similar indicating similar pulse shapes. The differences in the background between the resonances can be attributed to the finite interval for the FFT and to neglecting any noise in the model calculations.

4 Role of the Phase Current

Besides the discussed spectral position of the dispersive reflector, an appropriate phase of the light reflected back into the gain section is required for DQS-SP.
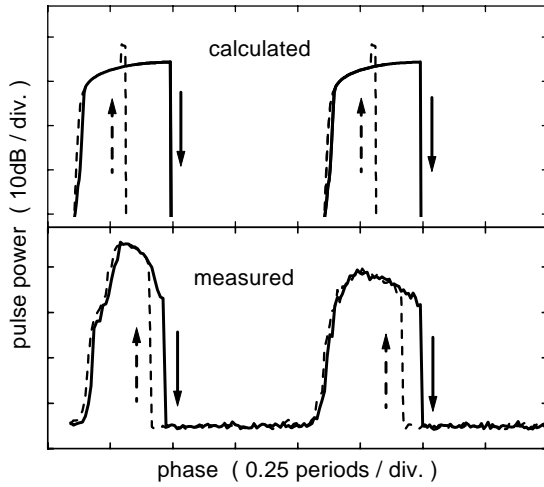
Fig. 4: Influence of the phase tuning on the pulse power. Full: increasing the phase tuning current. Dashed: decreasing the phase tuning current. Measured: height of the first peak in the rf spectrum. Calculated: modulation depth of the output power pulse trace.

Experimentally, the measured rf spectra show that SP can be switched on and off nearly periodically by changing the current through the phase tuning section [20]. Using the height of the first rf peak as a measure for the pulse power, the first two periods are plotted in Fig. 4. For an easier comparison with calculations, the relative number of periods is used as abscissa. The nonlinear relation between phase current and the phase was determined from a measurement in which the wavelength of the lasing mode was plotted as a function of the phase current. Consecutive intervals of wavelength jumps were used as indication of a 2π interval. SP are observed for approximately one third of each period.

The shapes of the SP regions are clearly asymmetric. A steep but smooth increase of the pulse power can be observed at the low phase borders. In contrast, the high phase borders show abrupt behavior of the pulse power and a distinct hysteresis.

The modeling is based on the following specific considerations for the phase tuning section. The gap wavelength $1.3\,\mu m$ of the waveguide material is much shorter than the $1.57\,\mu m$ operation wavelength. No stimulated interband transitions take place and we have $g = 0$ independent of N. Simulating this situation in our model by $g' = 0$, only the static contributions to β remain. The real part introduces the additional phase shift $\varphi_p = 2\delta_p l_p$ for the light traveling two times per round trip along the length l_p of the phase section. Tuning of the phase current causes changes of the carrier density in the phase section. This modifies in turn the effective refractive index of the waveguide, and, via δ_p, the phase shift φ_p. At the same time, also the

7

optical losses α_0 vary due to the free carrier absorption. Earlier measurements [19] have shown that α_0 changes by only about $5\,cm^{-1}$ per phase period. We do not take into account this weak correlation but treat φ_p and α_0 as independent parameters in the modeling.

The basic features of the role of the phase section calculated using these assumptions agree quite well with the measured features (Fig. 4):

(i) Phase tuning switches on and off the self-pulsations.

(ii) The SP appear for approximately a third of the phase period.

(iii) The width of the SP region depends however on the direction of the phase change.

(iv) This hysteresis appears only on the right side of the SP region, whereas the left side remains insensitive to the direction of the phase change.

Some differences in the details can be explained by simplifications of the model and by uncertainties of some parameters. No noise floor between the SP regions appears in the theory because all noise sources have been neglected. The calculated hysteresis is more pronounced than in the measurements. This is probably due to the neglected gain dispersion to be discussed below. Within the SP regions, the calculated pulse power increases monotonously, whereas the measured one exhibits a maximum. This slight difference may be due to the differing definitions of 'pulse power' given in the caption of Fig. 4. Finally, the theory is strongly periodic because all parameters but the phase angle φ_p are kept fixed. The measured widths of the SP regions raise a bit from period to period due to the increasing free carrier absorption discussed above. In the following, we shall focus on the second period.
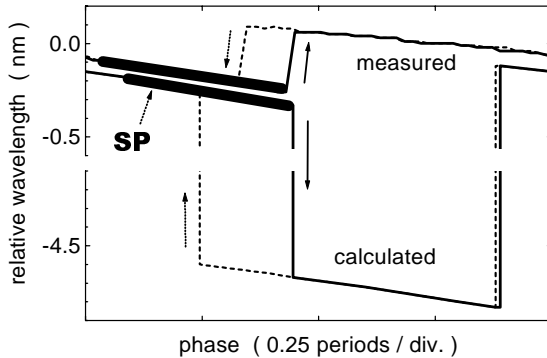
Fig. 5: Influence of the phase tuning on the emission wavelength for the second period of Fig. 4. Fat portions of the lines: Center of gravity of the broadened optical spectra in the self-pulsating regimes.

Changing the phase is further accompanied by some tuning of the emission wavelength λ as displayed in Fig. 5. Again, some features of the model agree well with the measurements:
(i) Extended regions of continuous shift are separated by points of wavelength jumps.
(ii) λ falls with increasing phase in the continuous regions. The slopes of this blue shift agree (about -0.3 nm per period).
(iii) the left border of the SP region is within a range of continuous shift, whereas the right border is connected with a wavelength jump.

Disagreement, however, is observed concerning the jumps of λ. The measured wavelengths show only one jump per cycle by about $+0.3\,nm$ compensating the continuous red-shift of the cycle. The model shows two jumps per cycle: one jump by

8

$-4.3\,nm$ from a self-pulsating long wave DFB mode across the stop band into a stationary state of the short wave DFB mode and another jump back between stationary states. Although some measured devices have also shown such mode jumps, they are much more pronounced in the calculations. We attribute this difference to the suppression of the short wave mode by the gain dispersion, which is not contained in the TWE-model. We tried to simulate an effective gain dispersion by using some numerical filtering technique which was suggested in [24]. This allowed indeed to suppress the short wave mode but we do not know yet whether the chosen parameters are realistic. Unfortunately, the proper consideration of dispersion requires a considerable extension of the model by adding at least one additional equation of motion for the dispersive polarization contribution to β. Therefore, we postpone this problem to further work. All further results of computations in this paper were obtained without gain dispersion focussing on cases with the long wave mode oscillating.

5   Roles of the Gain Current

Experimentally, the magnitude of the gain section current plays two major roles. In a first step it is used to adjust the wavelength of the lasing mode to a point on the decaying border of the reflectors stop band as indicated in Fig. 2, already discussed in chapter 3. Since the decaying border has a finite width, this can be achieved within a certain range of currents, which we call SP-island. The second role of the gain current is to change the properties of the SP, especially the pulsation frequencies, within the island.

Within the model, the gain current acts via two different terms. The first one is the injection term of the carrier rate equation (5). Secondly, the gain current acts indirectly via the heating of the gain section on the static thermal detuning δ between the two DFB sections. For separating the role of these two effects, we treat δ as an independent parameter in the model calculations of this chapter.

5.1   Role of detuning

For clarifying the role of the detuning effect, we have varied δ while fixing the gain section current (injection term) to a moderate value $I_g = 90$ mA. For a certain δ, the phase was increased stepwise. Fig. 6 shows the obtained SP-islands in the plane spread by the phase and the detuning. The total width of the island is about $0.5\,nm$. This corresponds to extension of the decaying slope of the reflectors reflectivity (cf. Fig. 2). The slope of the calculated SP island is correlated with the combined dispersion of the phase and reflector sections. In our example it is not much smaller than the round trip dispersion 1.2 phase periods per nm of the phase tuning section. It increases with increasing phase section length. For comparison with the experiment we have carried out the following measurements:

9
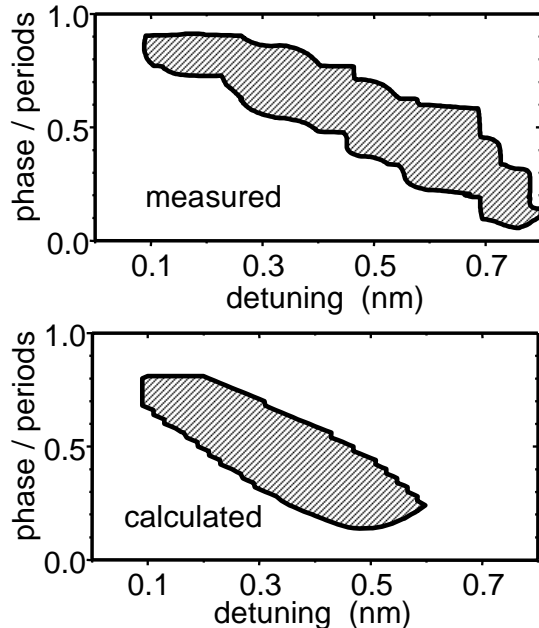
Fig. 6: Measured and calculated areas of high pulsation power as function of two parameters: 1. detuning of laser section (nm) with respect to the reflector and 2. detuning in the phase section (in periods). The detuning in the laser section originates from the temperature change due to increasing laser current. Injected current into gain section was 90 mA for the calculated results.

The reflector current was fixed for this measurement to $13\,mA$. Next the laser current was increased in $10\,mA$ steps from $50\,mA$ to $120\,mA$. For each laser current the phase current was tuned from 0 to $12\,mA$ which corresponds to about 2 cycles of 2π in phase. All regions in which the rf power is $> -30\,dBm$ are indicated as "pulsation". The relation between the laser current and the thermal detuning was measured with the same device. We plotted the spectral position of the non-pulsating laser mode for a range of the laser current from $50\,mA$ to $110\,mA$. It changes by about $0.7\,nm$ which is $4.2\,nm \cdot \mu m/mA$ for the $300\,\mu m$ long section which is in good agreement with previous measurements. The determined detuning was used as the abscissa value of fig. 6b. The measured island is very similar to the calculated one. Because the latter one was calculated for *constant* injection level, we can conclude that the width and position of the SP islands is determined mainly by the detuning parameter δ, whereas the injection level is of minor influence.

Our calculations show that this situation is rather insensitive to changes of the injection current due to the following effect. Increasing the current causes a certain primary thermal red shift, which reduces the feedback from the reflector. The laser responses by increasing the carrier density, which is accompanied by an electronic blue-shift. As a consequence, the resulting wavelength shift is much smaller than the primary thermal red-shift.

5.2 Role of the injection level

SP frequency is affected mainly by the injection level but only marginally by the detuning as shown in Fig. 7.

We measured the influence of the laser current on the SP frequency in such a way that the device remains in the pulsation state when the current I_g is changed from $60\,mA$ to $110\,mA$. This situation can be obtained by reducing the phase current for this specific device according to the linear relation

$$I_p = 5.562 - 0.0505 I_g \tag{8}$$

10

when the laser current is increased. With this correlation a trajectory in the centre of the pulsation island of Fig. 6 is passed through. The continuous SP frequency ranges at least from 7 to $10\,GHz$ for this parameter set.
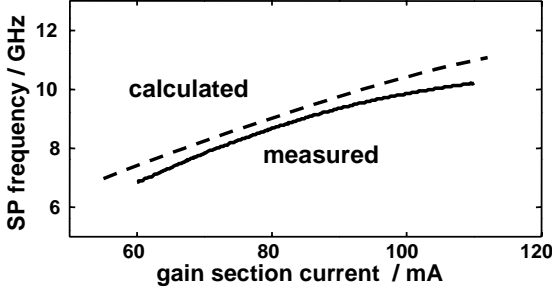
Fig. 7: Measured pulsation frequency as a function of the increasing laser current. The phase current is reduced at the same time in order to keep the pulsation amplitude high. Thus the operation parameters always remain in the areas shown in fig. 7 Shown are also calculated results with different values of the gain detuning. This demonstrates the small influence of the detuning on the pulsation frequency. In the experimental curve the effect of injection current and detuning cannot be distinguished.

The measured and calculated SP frequency has a square root law dependence on the difference between injection and threshold current:

$$f_{SP} \propto \sqrt{(I - I_{th})}. \tag{9}$$

This can be understood if we assume that SP occurs just at the frequency of the relaxation oscillations but with an additional mechanism for undamping being present. The relaxation oscillations depend not only on the photon number and differential gain as for ordinary single section DFB-lasers but can also be tuned by a dispersive reflector. In this case we obtain:

$$f_{relax} = \frac{1}{2\pi}\sqrt{(\gamma_m + \gamma_i)S\frac{\partial(\Gamma G - \gamma_m)}{\partial N}}. \tag{10}$$

Here γ_m is the mirror loss, γ_i are the internal loss, S the photon number, N the carrier density Γ is the confinement factor and G is the gain of the active section.
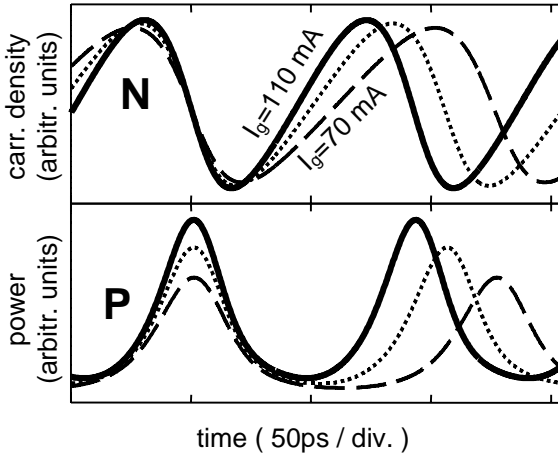
Fig. 8: Temporal variation of carrier density and optical power for different levels of injection.

Depending on the sign of $\frac{\partial \gamma_m}{\partial N}$, f_{relax} will increase or decrease. An explanation of the SP-frequency dependence upon injection current can be given as follows. During a period of SP we have an increase of photon number S. This increased number reduces the carriers and shifts the laser oscillation to higher wavelengths. Now we have less reflectivity together with reduced carrier density and the laser is switched off. By carrier injection the laser threshold is reached again and the laser is switched on. The higher the injection level the shorter is the gain recovery time.

This can be clearly observed in Fig. 8. The shape of the individual pulses, however, remain nearly unchanged. We also like to emphasize the fact that this paper covers only passive reflectors (operation close to transparency). Higher frequency SP are

obtainable with different operation conditions of the reflector mirror.

6   Conclusion

A comprehensive and effective model of a 3-section laser with integrated phase tuning section has been proposed. The particular parameter configuration of a device which had been successfully applied in optical transmission experiment served as test vehicle for the model. Very good agreement between theory and experiment has been shown. Those parameters in which discrepancy occurred were discussed in the paper and require an extension of the model. The actual version is ready to be used to optimise the 3-section laser. Its use as clock recovery is at present the most important application of the self-pulsating laser. With this model we will be able to optimise features like pulsation-frequency, area of pulsation island locking to injected signals as a function of different device parameters such as section lengths, differential gain of the active layer, detuning between laser and reflector and grating structure.

References

[1] M. Möhrle, U. Feiste, J. Hörer, R. Molt, and B. Sartorius, "Gigahertz self-pulsations in 1.5 μm wavelength multisection DFB lasers," *IEEE Photon. Technol. Lett.* **4**, pp. 976-979, 1992.

[2] B. Sartorius, M. Möhrle, and U. Feiste, "12 GHz to 64 GHz continuous frequency tuning in self-pulsating 1.55 μm multi quantum well DFB lasers," IEEE J. of Selected Topics in Quantum Electronics 1, pp. 535-38, 1995.

[3] B. Sartorius, M. Möhrle, and S. Reichenbacher, "Wavelength and polarization independent synchronization of high frequency DFB type self-pulsations", Electron. Lett. 32, pp. 1026-28, 1996.

[4] B. Sartorius, M. Möhrle, and S. Reichenbacher, "Wavelength independent clock recovery at 10 Gb/s using self-pulsating DFB lasers with integrated phase tuning section", accepted for ECOC '96.

[5] B. Sartorius, C. Bornholdt, O. Brox, H. J. Ehrke, D. Hoffmann, R. Ludwig, and M. Möhrle, "All-optical clock recovery module based on a self-pulsating DFB laser," *Electron. Letters* **34**, pp. 1664-65, 1998.

[6] B. Sartorius, C. Bornholdt, O. Brox, H.J. Ehrke, D. Hoffmann, R. Ludwig, and M. Möhrle: "System performance of an all-optical clock recovery module" ECOCʹ98, Madrid, Conf. Proc. pp.505-506, 1998.

[7] A. Buxens, A.T. Clausen, H.N. Poulsen, K.S. Jepsen, K.E. Stubkjaer, C. Born-holdt, O. Brox, and B. Sartorius: 40 to 10 Gb/s demultiplexing using a self-pulsating DFB laser for clock recovery, ECOC'98, Madrid, Conf. Proc. pp.507-508, 1998.

[8] P. Phelan, D. McDonald, A. Egan, J. Hegarty, R. O'Dowd, G. Farrell, and S. Lindgren, "Comparison of self-pulsation in multisection lasers with distributed feedback and intracavity saturable absorbers," *Proc. Inst. Elect. Eng.* **141**, pp. 114-118, 1994.

[9] A.-J. Lowery and P. C. R. Gurney, "Improving pulses from 2-contact self-pulsating DFB semiconductor lasers," *Conf. Dig. 14th IEEE Int. Semicond. Laser Conf.*, Hawaii, pp. 103-104, 1994.

[10] G.-H. Duan and P. Landais, "Self-pulsation in multielectrode distributed feed-back semiconductor lasers," Proc. 10th int. Conf. Integrat. Optics and Optical Fiber Commun., Hongkong, pp. 132-133, 1995.

[11] R. Schatz, "Longitudinal spatial instability in symmetric semiconductor lasers due to spatial hole burning," *IEEE J. Quantum Electron.*, vol. QE-28, pp. 1443-1449, 1992

[12] A. J. Lowery, "Dynamics of SHB-induced mode instabilities in uniform DFB semiconductor lasers,"*Electron. Lett.*, vol.29, pp. 1852-1854, 1993.

[13] D. D. Marcenac and J. E. Caroll, "Distinction between multimoded and sin-glemoded self-pulsations in DFB lasers," *Electron. Lett.*, vol.30, pp. 1137-1138, 1994.

[14] U. Bandelow, H.-J. Wünsche, and H. Wenzel, "Theory of self-pulsations in two-section DFB lasers," *IEEE Photon. Technol. Lett.*, vol. 5, pp. 1176-1179, 1993.

[15] H.J. Wünsche, U. Bandelow, H. Wenzel and D. Marcenac, "Self pulsations by mode degeneracy in two-section DFB lasers", *SPIE Proceedings Series*, vol. 2399, pp. 195-206, 1995.

[16] H. Wenzel, U. Bandelow, H.J. Wünsche and J. Rehberg, "Mechanisms of fast self pulsations in two-section DFB lasers", *IEEE J. Quantum Electron.*, vol. 32, pp. 69-79, 1996.

[17] B. Sartorius, M. Möhrle, S. Reichenbacher, and W. Ebert "Controllable self-pulsations in multisection DFB lasers with an integrated phase-tuning section," *IEEE Photon. Technol. Lett.*, vol. 7, no. 11, pp. 1261-1263, 1995.

[18] B.Sartorius, M. Möhrle, S. Reichenbacher, H. Preier, H.-J. Wünsche, and U. Bandelow "Dispersive self Q-switching in self-pulsating DFB lasers," submitted to *IEEE J. Quantum Electron.*

[19] U. Bandelow, H.J. Wünsche, B. Sartorius and M. Möhrle "Dispersive Self-Q-Switching in DFB Lasers – Theory Versus Experiment", *IEEE J. Selected Topics in Quantum Electronics*, vol. 3, No. 2, pp. 270-278, 1997.

[20] M. Möhrle, B. Sartorius, R. Steingrüber, and P. Wolfram, "Electrically switchable self-pulsations in integrable multisection DFB-lasers", *IEEE Photon. Technol. Lett.*, vol. 8, no. 1, pp. 28-30, 1996.

[21] M.G. Davis and R.F. O'Dowd, "A new large-signal dynamic model for multi-electrode DFB lasers based on the transfer matrix method", *IEEE Phot. Techn. Lett.*, vol. 4, pp. 838-840, 1992.

[22] L.M. Zhang, S.F. Yu, M.C. Nowell, D.D. Marcenac, J.E. Carroll and R.G.S. Plumb, "Dynamic Analysis of Radiation and Side-Mode Suppression in a Second-Order DFB Laser Using Time-Domain Large-Signal Traveling Wave Model", *IEEE J. Quantum Electron.*, **30**, No. 6, pp. 1389-1395, 1994.

[23] L.M. Zhang and J.E. Carroll, "Large-signal dynamic model of DFB laser", *IEEE J. Quantum Electron.*, vol. 28, pp. 604-611, 1992.

[24] D. Marcenac, "Fundamentals of laser modelling", *Doctoral dissertation, St. Catharine's College, University of Cambridge*, 1993.

[25] B. Tromborg, H.E. Lassen, H. Olesen, and X. Pan, "Traveling wave method for calculation of linewidth, frequency tuning, and stability of semiconductor lasers," *IEEE Photon. Techn. Lett.*, vol. 4, 985-988, 1992.